ELSEVIER

Biophysical Chemistry 105 (2003) 721–741

Biophysical Chemistry

www.elsevier.com/locate/bpc

Studies of short-wavelength collective molecular motions in lipid bilayers using high resolution inelastic X-ray scattering☆

Poe-Jou Chen[a], Yun Liu[a], Thomas M. Weiss[b], Huey W. Huang[b], Harald Sinn[c], Ercan E. Alp[c], Ahmet Alatas[c], Ayman Said[c], Sow-Hsin Chen[a,*]

[a]*Department of Nuclear Engineering, Massachusetts Institute of Technology, 24-209, MIT, Cambridge, Massachusetts 02139, USA*
[b]*Physics Department, Rice University, Houston, Texas 77251-1892, USA*
[c]*Advanced Photon Source, Argonne National Laboratory, Argonne, IL 60439, USA*

Received 9 November 2002; received in revised form 3 March 2003; accepted 3 March 2003

Abstract

We summarize a series of experimental results made with the newly developed high resolution X-ray scattering (IXS) instrument on two pure lipid bilayers, including dimyristoylphosphatidylcholine (DMPC) and dilauroylphosphatidylcholine (DLPC) in both gel and liquid crystal phases, and lipid bilayers containing cholesterol. By analyzing the IXS data based on the generalized three effective eigenmode model (GTEE), we obtain dispersion relations of the high frequency density oscillations (phonons) of lipid molecules in these bilayers. We then compare the dispersion relations of pure lipid bilayers of different chain lengths among themselves and the dispersion relations of pure lipid bilayers with those of the cholesterol containing bilayers. We also compare our experimental results with collective dynamics data generated by computer molecular dynamics (MD) simulations for dipalmitoylphosphatidylcholine (DPPC) in gel phase and DMPC in liquid crystal phase.

Keywords: Collective dynamics in lipid bilayers; Inelastic X-ray scattering; Phonon dispersion relations; Generalized three effective eigenmode theory

1. Introduction

Biological membranes play a significant role in a range of biological processes such as ion-transport and signal transduction. All biological membranes are composed of mixtures of several lipids and of specific amphiphilic proteins [1]. But in the native state, the biological membrane is difficult to study. Cell membranes and vesicles are not in states which could be easily manipulated for investigation. As a result, phospholipid bilayers will be used as a model system for our study. Fully hydrated phospholipid bilayers have been employed as a model system in many biological studies to provide insight into the structure and function of biological membranes that has proven to be very successful.

☆ Contribution to a special issue of *Biophysical Chemistry* in honor of Professor Emeritus Walter Kauzmann.

*Corresponding author. Tel.: +1-617-253-3810; fax: +1-617-258-8863.
E-mail address: sowhsin@mit.edu (S.-H. Chen).

0301-4622/03/$ - see front matter © 2003 Elsevier Science B.V. All rights reserved.
doi:10.1016/S0301-4622(03)00099-1

Because of their amphiphilic characters, consisting of a polar head and a bulky hydrophobic double chain of hydrocarbon groups in the tail region, these lipids are known to readily self-assemble into ordered bilayers and depending on the temperature, exhibit different structural phases [2]. The structures of phospholipid bilayers have been studied by a variety of methods, such as differential scanning calorimetry [3], H^2 nuclear magnetic resonance [4,5], X-ray and neutron diffractions [6–8], and computer molecular dynamics simulations [9–11]. For the single particle dynamics, the diffusion and rotation of lipid molecules in bilayers have been studied by ESR [12], NMR [13,14], excimer [15] and by fluorescence recovery after photo-bleaching [16]. A recent incoherent quasi-elastic neutron scattering experiment [17] measured the confined diffusion of lipid molecules in oriented DPPC bilayers by time of flight and back-scattering neutron spectroscopy. Also, the undulatory low frequency excitations of highly ordered stacks of chain-deuterated lipid bilayers at a high hydration level have been studied by coherent neutron spin–echo spectroscopy [18]. However, studies of the in-plane collective dynamics of lipid chains are scarce so far [19,20]. Knowledge of collective density fluctuation of hydrocarbon chains in lipid bilayers is essential for understanding some aspects of biological functions of natural membranes. For example, it has been conjectured that the formation of gauche-trans-gauche kinks due to the collective thermal motion of hydrocarbon chains provides a possibility for the transmembrane transport of small molecules such as water or ions [23].

From the experimental point of view, the measurement of dynamic structure factor $S(k,\omega)$ is used to study the collective excitations in condensed matter. In the past, $S(k,\omega)$ has been studied extensively by Brillouin light scattering (BLS) and inelastic neutron scattering (INS) techniques. In INS, the small-k range is not accessible due to the kinematic limitation related to the neutron mass and one is unable to observe the collective excitations of long wave lengths because of the limited accessible $k-\omega$ ranges. As for BLS, because of the long wavelength of light, it limits the accessible k range to $k<0.01$ nm^{-1}.

The k range, inaccessible by the aforementioned experimental techniques ($1\ \text{nm}^{-1}\leq k\leq 5\ \text{nm}^{-1}$), is important for the understanding of the collective dynamics. In order to measure the speed of sound, we need a linear region of the phonon dispersion curve for the measured k range, and the same k range also corresponds to wave vector transfer near the inverse of the inter-particle distance ($k=1-15\ \text{nm}^{-1}$), where the collective dynamics goes through a transition from a hydrodynamics to a microscopic single-particle behavior.

The rapid development of synchrotron radiation sources make the IXS technique that could cover the missing k range feasible only happened in recent years. In 2000, Chen et al. [19] made the first measurement of collective dynamics in DLPC phospholipid bilayers and obtained some results, which showed a good agreement with the later MD simulation by Tarek et al. [20]. However, in these articles, they only studied the dynamics of pure lipids. In real biological system, membranes are not pure lipid bilayers. For example, cholesterol plays in many ways ubiquitous role in biological membranes where it can account for up to 50 mol.% of the total lipids in the cell membranes. The presence of cholesterol is required for mammalian plasma membranes to function normally. Although cholesterol has a number of different functions, it is important as a modulator of the physical and transport properties of the plasma membrane and is necessary for the functional activity of several membrane protein [21]. For instance, adding cholesterol to a lipid bilayer enhances its bending elasticity [22] and reduces its passive permeability [23,24].

Moreover, it is also known that cholesterol reduces order in gel phase bilayers and increases order in liquid crystal phase bilayers, hence broadening or even eliminating the main bilayer phase transition. When in the case of high cholesterol concentration, cholesterol increases the mechanical strength, lowers the permeability and suppresses the main-phase transition. On the other hand, at low concentration and close to the main phase transition temperature, cholesterol, instead of enhancing the strength, softens the bilayer and increases its permeability. It has been shown that adding cholesterol to phospholipid membranes pro-

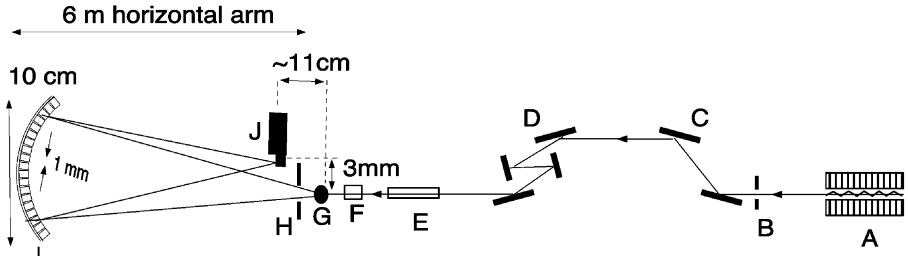

Fig. 1. The schematic diagram of an inelastic X-ray scattering spectrometer at Beamline 3-ID, Advanced Photon Source and Argonne National laboratory. The beam comes from an undulator (A) and pre-monochromator (C), then passes through the high-resolution monochromator (D) and focusing mirror (E) before it illuminates the sample (G). The scattering intensity is focused by analyzer (I) into detector (J). (F) is the ionization chamber to monitor the incident flux onto sample. (B) and (H) are the slit systems that determine the source size.

duces a rich phase diagram of the mixer. In Vist and Davis's article [25], they mapped out such phase diagram for dipalmitoylphosphatidylcholine (DPPC)/cholesterol in the presence of water. They showed that by adding a substantial amount of cholesterol to DPPC membranes, a new phase that is different from gel and liquid crystal is formed with the properties of a liquid and solid. In Zuckermann's article [26], the new phase is called a solid–liquid-ordered phase according to the new classification scheme introduced by them, while the gel phase is called solid-ordered phase and in the liquid crystal phase is called liquid-ordered phase. When the cholesterol level is low, we can find the usual two phases: solid- and liquid-ordered and there is a transition temperature. When there exists substantial amount of cholesterol in DPPC, the liquid-ordered phase is present but we can't observe the solid-ordered phase by lowering the temperature. Though a lot of efforts has been put into the understanding of the properties of phospholipid membranes in the presence of cholesterol [27–32], the studies of its in-plane collective dynamic is still much needed.

MD simulation of phospholipid bilayers can help interpret the IXS data since the k and ω values accessible to both techniques are about the same. In this article, we will summarize the new results obtained from the recent study of the collective dynamics of the lipids with the addition of cholesterol [33] by coherent inelastic X-ray scattering and will also compare these new results with Chen's previous article [19] and also the available MD data [20].

2. The IXS experiment

The experiment for DMPC and DMPC with cholesterol was carried out at the high resolution inelastic X-ray scattering beam line (3-ID) at the Advanced Photon Source (APS). Fig. 1 is the schematic diagram of the inelastic X-ray scattering spectrometer at the Advanced Photon Source, Argonne National laboratory. The 21.657 keV (denoted by E_1) X-ray was produced by a 4.6 m long undulator with a 2.7 cm magnetic period at the storage ring of the APS at Sector 3 [34]. The beam was pre-monochromated by a water-cooled diamond (1 1 1) double-crystal monochromator. It is further monochromatized by a high resolution in-line monochromator, which consists of two nested silicon channel-cut crystals. An asymmetrically cut silicon (4 4 0) crystal is used as the outer channel of the in-line monochromator. It is able to collimate the incoming beam to below one microradian inside the channel cut. After the outer crystal, the beam is reflected twice by the inner channel cut with a Bragg angle at 83.2° at the (15 11 3) reflection. After transmitting through the second monochromator, the beam has a tunability range between 21.50 and 21.70 keV with an energy width of 1.3 meV. By rotating the inner and outer channel-cut of the in-line monochromator, we can tune the energy on the meV scale. The beam is

then focused by a total reflecting mirror to a spot size at the sample of 200×100 μm after passing through the high energy resolution monochromator. The photon flux at the sample position is approximately 6×10^8 photons/s at a current of 100 mA in the storage ring.

The scattered photon was collected by a (18 6 0) reflection of a bent silicon analyzer in extreme back-scattering geometry ($\theta_B=89.98°$). The analyzer is comprised of a 4 mm thick, 100 mm large focusing silicon disk, with a distance of 6 m from the sample. The disk is glued onto a flexible glass wafer and diced with a high-precision diamond saw into small pixels of 1 mm size in order to avoid bending stress in the silicon. By etching the crystal in a KOH solution, the stress from distorted areas at the cut regions can be removed.

A temperature-controlled chamber is used to house the analyzer to keep the temperature stabilized near room temperature to ±2 mK/24 h.

A commercially available Cd–Zn–Te semiconductor detector is used here. Its electronic noise level is below 0.001 Hz.

The wavevector transfer, k, can be varied according to the relation

$$k=\frac{4\pi}{\lambda}\sin\frac{\theta}{2}=21.95\ \text{Å}^{-1}\sin\frac{\theta}{2} \quad (1)$$

where λ is the wavelength of the X-rays and θ the scattering angle at the sample. The maximum scattering angle of the setup is $\theta\leq15.5°$, which corresponds according to the above equation to a maximum momentum transfer of 30 nm^{-1}.

The net energy resolution function was measured by a Plexiglas sample with a 1.97 meV full width at half maximum. The shape of the measured resolution function can be reasonably well described by a fit with a Pseudo–Voigt function

$$I(\omega)=I_o\left\{\frac{2\eta}{\pi\Gamma}\left[1+\left(\frac{\omega}{\Gamma}\right)^2\right]^{-1}+(1-\eta)\frac{2}{\Gamma}\times\left(\frac{\ln2}{\pi}\right)^{1/2}\times\exp\left[-4\ln2\left(\frac{\omega}{\Gamma}\right)^2\right]\right\} \quad (2)$$

where $\Gamma=1.97$ meV is the full half maximum value of the curve, $\eta=0.65$ the mixing parameter and I_o a normalization constant.

Lipid bilayer samples were fully hydrated films of thinkness approximately 1 mm and area 1 cm^2 deposited on a quartz plate. They were placed in an air–tight aluminum rectangular box with capton windows. The incoming X-ray beam enters horizontally, parallel to the plane of the sample and the scattered beam is collected also in the horizontal direction so that the scattering plane coincides with the plane of the sample. By this way, we can assure that scattering vector k is largely in the plane of lipid bilayers. The path length of the X-ray in the sample is approximately 1 cm.

3. Theoretical model

Atomic and molecular density fluctuations of simple fluids have been studied extensively both experimentally and theoretically in the past two decades [35–37]. In Born approximation, the double differential cross sections of both inelastic photon and neutron scattering from simple fluids are proportional to the dynamic structure factor $S(k,\omega)$, where k is the magnitude of the wave vector transfer (see Eq. (1)) and $\hbar\omega$ ($E=\hbar\omega=E_1-E_2$, where E_1 and E_2 are the incident and scattered energies of the radiation, respectively) the energy transfer in the scattering process [38]. $S(k,\omega)$ is the density fluctuation of the atomic or molecular density in the fluid. This gives an incentive for formulating a dynamical theory of fluid which contains explicitly the dynamic structure factor which is measured in an IXS scattering experiment. The IXS data were analyzed by a generalized three effective eigenmode model (GTEE), developed in a recent article by Liao and Chen [39]. They extended a three effective eigenmode model (TEE) formulated previously by de Schepper and co-workers for simple liquids to supramolecular liquids [40–43]. Generally speaking, GTEE is a direct extension of the macroscopic hydrodynamic theory [35], including three k-dependent quasi-hydrodynamic modes, namely, the number density, the longitudinal current density and the energy density. In this section, we will briefly describe the GTEE model and discuss the method of analysis of the IXS data.

3.1. Generalized dynamic structure factor

In a scattering experiment, each target particle converts the incident plane wave into a spherical scattered wave with a specific amplitude. The scattering amplitude of each scattering particle is generally k-dependent. In IXS, the scattering amplitude of the particle (atom) is proportional to $r_o f_i(k)$ where r_o denotes the classical radius of electron, and $f_i(k)$ the form factor of the scattering atom with index i. The form factor is normalized in such a way that it is equal to the atomic number Z when k equals to zero. One can find the tabulated values of the form factors for different atoms in International Tables for X-ray Crystallography [44]. The double differential cross-section for IXS from a sample containing N atoms is formally written as [38].

$$\frac{\mathrm{d}^2\sigma}{\mathrm{d}\Omega\mathrm{d}E} = Nr_o^2(\varepsilon_i\cdot\varepsilon_f)^2\frac{k_f}{k_i}\frac{1}{N} \times \sum_{F_n,I_n} P_{\mathrm{In}}\left|\left\langle F_n\left|\sum_j^N f_j(k)\mathrm{e}^{i\mathbf{k}\cdot\mathbf{r}_j}\right|I_n\right\rangle\right|^2 \times \delta(E-E_f+E_i), \tag{3}$$

where E denotes the energy transfer of an X-ray photon to the medium in the scattering process and ε the polarization of the X-ray. The indexes i,f denote the incident and scattered X-rays, respectively. I_n,F_n are the initial and final states of the system in the scattering process. P_{In} is the probability that the system is in the initial state I_n.

One can define the dynamic structure factor measured by IXS as

$$S(k,E) = \frac{1}{N}\sum_{F_n,I_n} P_{\mathrm{In}}\left|\left\langle F_n\left|\sum_j^N f_j(k)\mathrm{e}^{i\mathbf{k}\cdot\mathbf{r}_j}\right|I_n\right\rangle\right|^2 \times\delta(E-E_f+E_i) \tag{4}$$

$$S(k,E) = \frac{1}{2\pi\hbar}\frac{1}{N}\int \mathrm{d}t\ \mathrm{e}^{iEt/\hbar} \times \sum_{j,l}^N \langle f_i(k)f_l(k)\mathrm{e}^{i\mathbf{k}\cdot\mathbf{r}_l(0)}\mathrm{e}^{-i\mathbf{k}\cdot\mathbf{r}_j(t)}\rangle. \tag{5}$$

The defined dynamic structure factor takes into account the atomic form factors. The double differential cross section can then be written as

$$\frac{\mathrm{d}^2\sigma}{\mathrm{d}\Omega\ \mathrm{d}E} = Nr_o^2(\varepsilon_i\cdot\varepsilon_f)^2\frac{k_f}{k_i}S(k,E). \tag{6}$$

We shall, in the following, use the notation $S(k,\omega)=\hbar S(k,E)$. The intermediate scattering function (ISF) is the inverse Fourier transform of the dynamics structure factor $S(k,\omega)$,

$$F(k,t) = \frac{1}{N}\sum_{j,l}\langle f_j(k)f_l(k)\mathrm{e}^{-i\mathbf{k}\cdot\mathbf{r}_l(0)}\mathrm{e}^{i\mathbf{k}\cdot\mathbf{r}_j(t)}\rangle. \tag{7}$$

Introducing now the extended density fluctuation $n(k,\ t)$ by including the form factor as

$$n(k,t) = \frac{1}{\sqrt{N}}\sum_j f_j(k)\mathrm{e}^{-i\mathbf{k}\cdot\mathbf{r}_j(t)} \tag{8}$$

we have

$$F(k,t) = \langle n^*(k,0)n(k,t)\rangle. \tag{9}$$

In our experiment, fully hydrated lipid molecules can be seen as a kind of complex fluids composed of more than one type of atoms, it is advantageous to decompose the above defined dynamic structure factor into the weighted average of partial dynamic structure factors for all different types of atoms. This is accomplished by splitting the extended density fluctuation into the sum of the density fluctuation of each type of atom,

$$n(k,t) = \sum f_\alpha(k)\omega_\alpha n_\alpha(k,t) \tag{10}$$

where α denotes the type of atom, $\omega_\alpha=\sqrt{N_\alpha/N}$, the square root of the number fraction of atomic type α over the total atom number and $n_\alpha(k,\ t)$, the density fluctuation of the atom type α given by

$$n_\alpha(k,t) = \frac{1}{\sqrt{N_\alpha}}\sum_j^{N_\alpha}\mathrm{e}^{-i\mathbf{k}\cdot\mathbf{r}_j(t)}. \tag{11}$$

The prime in the last equation denotes that the sum is only over the different types of atoms within type α. By using Eq. (10), we can write:

$$F(k,t)=\sum_{\alpha,\beta}f_{\alpha}(k)f_{\beta}(k)\omega_{\alpha}\omega_{\beta}F_{\alpha\beta}(k,t), \tag{12}$$

where the partial intermediate scattering function is defined as:

$$F_{\alpha\beta}(k,t)=\langle n^{*}_{\alpha}(k,0)n_{\beta}(k,t)\rangle. \tag{13}$$

The Fourier transform relationship between the dynamic structure factor and the intermediate scattering function implies that the moments of the dynamic structure factor determine the short time behavior of $F(k, t)$. In particular, the static structure factor $S(k)$, is the initial value of ISF, $F(k, t=0)$. The generalized static structure factor $S(k)$ measured by an X-ray diffraction experiments is given as

$$S(k)=\langle n^{*}(k)n(k)\rangle=\frac{1}{N}\sum_{j,l}\langle f_{j}(k)f_{l}(k)\mathrm{e}^{i\mathbf{k}\cdot\mathbf{r}_{l}}\mathrm{e}^{-i\mathbf{k}\cdot\mathbf{r}_{j}}\rangle. \tag{14}$$

Insert Eq. (10) into the above equation, we have a useful representation of structure factor in the following

$$S(k)=\sum_{\alpha\beta}f_{\alpha}(k)f_{\beta}(k)\omega_{\alpha}\omega_{\beta}S_{\alpha\beta}(k) \tag{15}$$

where the partial structure factor $S_{\alpha\beta}(k)=\langle n^{*}_{\alpha}(k)n_{\beta}(k)\rangle$.

Likewise, the dynamic structure factor can also be written as a weighted sum over partial dynamic structure factor with the weights determined by the number fraction and atomic form factor of the pair. The dynamic structure factor can finally be written in a transparent way as:

$$S(k,\omega)=\sum_{\alpha\beta}f_{\alpha}(k)f_{\beta}(k)\omega_{\alpha}\omega_{\beta}S_{\alpha\beta}(k,\omega). \tag{16}$$

Since the atomic form factor is proportional to the atomic number of the element, in our experiment, the carbon–carbon and oxygen–oxygen partial structure factor ought to dominate both the static and dynamic structure factors. It turns out that the MD simulation [20] showed that in the case of fully-hydrated lipid bilayers, the dominating partial structure factors are the carbon–carbon one only because carbon atoms in the lipid molecules are much more ordered than oxygen atoms in hydration water molecules. This fortunate situation leads to the interpretation that the measured phonons are indeed coming from the density oscillation of the center of mass of the lipid molecules constituting the bilayer.

3.2. Generalized three effective eigenmode (GTEE) model

In the GTEE model, the correlation function matrix $\mathbf{G}(k,z)$ for the three slow microscopic fluctuations: number density (labeled as '*n*'), longitudinal velocity (labeled as '*u*') and energy density (labeled as '*T*'), obeys a hydrodynamic-like equation:

$$z\mathbf{G}(k,z)=\mathbf{H}(k)\mathbf{G}(k,z)+\mathbf{I}. \tag{17}$$

Then the dynamic structure factor is given as (we put $z=-i\omega$)

$$S(k,\omega)=\frac{S(k)}{\pi}\mathrm{Re}\left\{\frac{-\mathbf{I}}{i\omega+\mathbf{H}(k)}\right\}_{1,1}, \tag{18}$$

where $\mathbf{I}$ is the 3×3 identity matrix, label 1,1 outside the curly bracket means the (1,1) element of the matrix. The hydrodynamic matrix $\mathbf{H}$ is given in terms of four independent phenomenological k-dependent parameters,

$$\mathbf{H}(k)=\begin{pmatrix}0 & if_{un}(k) & 0\\ if_{un}(k) & z_{u}(k) & if_{uT}(k)\\ 0 & if_{uT}(k) & z_{T}(k)\end{pmatrix}, \tag{19}$$

where the matrix element $f_{un}(k)$ is the second frequency moment of the dynamic structure factor. It is given in terms of the structure factor $S(k)$, as

$$f_{un}(k)=kv_{o}(k)[S(k)]^{-1/2} \tag{20}$$

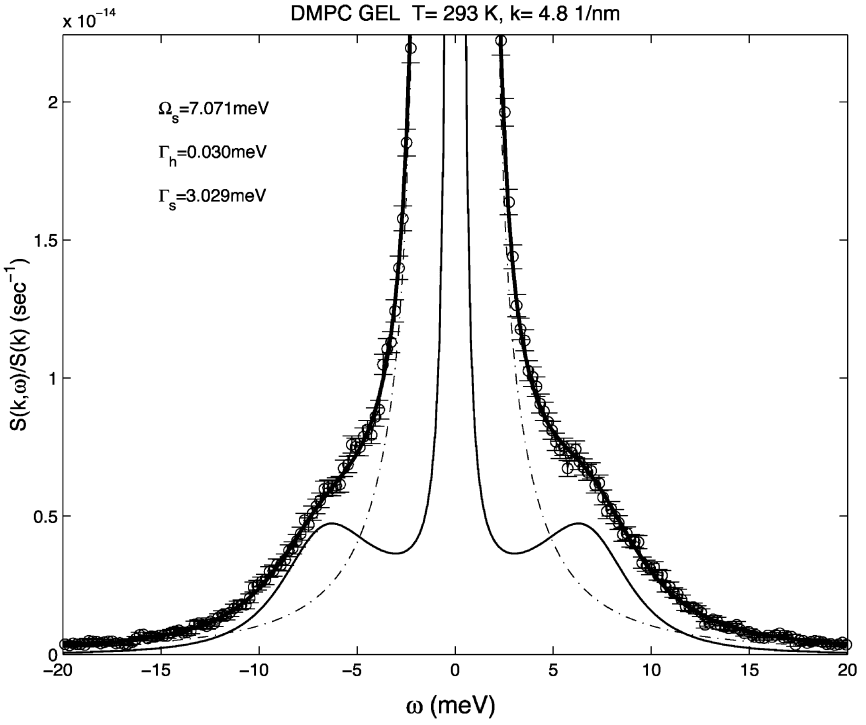

Fig. 2. A typical fit of the IXS spectra at $k=4.8$ nm^{-1} with the GTEE theory. The sample is a DMPC bilayer in the gel phase at $T=293$ K. The fit gives the width of the central peak, 0.03 meV, much less than the width of energy resolution function, the FWHM of which is 1.97 meV. The in-plane phonon frequency, $\Omega_s=7.071$ meV, is clearly resolved, giving the propagating sound speed of 2229.7 m/s. The damping of the phonon is 3.029 meV.

where the generalized thermal speed $v_o(k)$ is the weighted average of the thermal speeds $v_{o\alpha}=\sqrt{k_BT/M_\alpha}$ of different types of atoms present in the bilayer system defined as,

$$v_o^2(k)=\sum_\alpha f_\alpha^2(k)\omega_\alpha^2 v_{o\alpha}^2. \tag{21}$$

It should be noted here that from the fitted value of $f_{un}(k)$, we can deduce the absolute value of the generalized structure factor $S(k)$ (defined in Eq. (15) above) by calculating the generalized thermal speed according to Eq. (21). The other three independent parameters: $z_u(k)$, $f_{uT}(k)$, $z_T(k)$ are all real numbers and the small k limit of these three parameters is related to thermal dynamical and transport parameters of the fluid in a unique way [43].

One can rewrite Eq. (18) as:

$$S(k,\omega)/S(k)=-\frac{1}{\pi}\mathrm{Re}\left\{\frac{1}{\det(i\omega\mathbf{I}+\mathbf{H})}\mathrm{Adj}(i\omega\mathbf{I}+\mathbf{H})_{1,1}\right\} \tag{22}$$

where $\det(i\omega\mathbf{I}+\mathbf{H})$ is the determinant of the matrix $(i\omega\mathbf{I}+\mathbf{H})$, while $\mathrm{Adj}(i\omega\mathbf{I}+\mathbf{H})_{1,1}$ is the first element of the adjunct matrix of $(i\omega\mathbf{I}+\mathbf{H})$. After evaluating the matrix elements, it becomes

$$\frac{S(k,\omega)}{S(k)}=\mathrm{Re}\left\{\frac{S(k,z)}{S(k)}\right\}= -\frac{1}{\pi}\mathrm{Re}\left\{\frac{z^2-(z_u+z_T)z+z_uz_T+f_{uT}^2}{-z^3+(z_u+z_T)z^2-(z_uz_T+f_{uT}^2+f_{un}^2)z+f_{un}^2z_T}\right\} \tag{23}$$

where $-i\omega$ is replaced by z. If we put the numerator $z^2-(z_u+z_T)z+z_uz_T+f_{uT}^2$ as $P(z)$ and

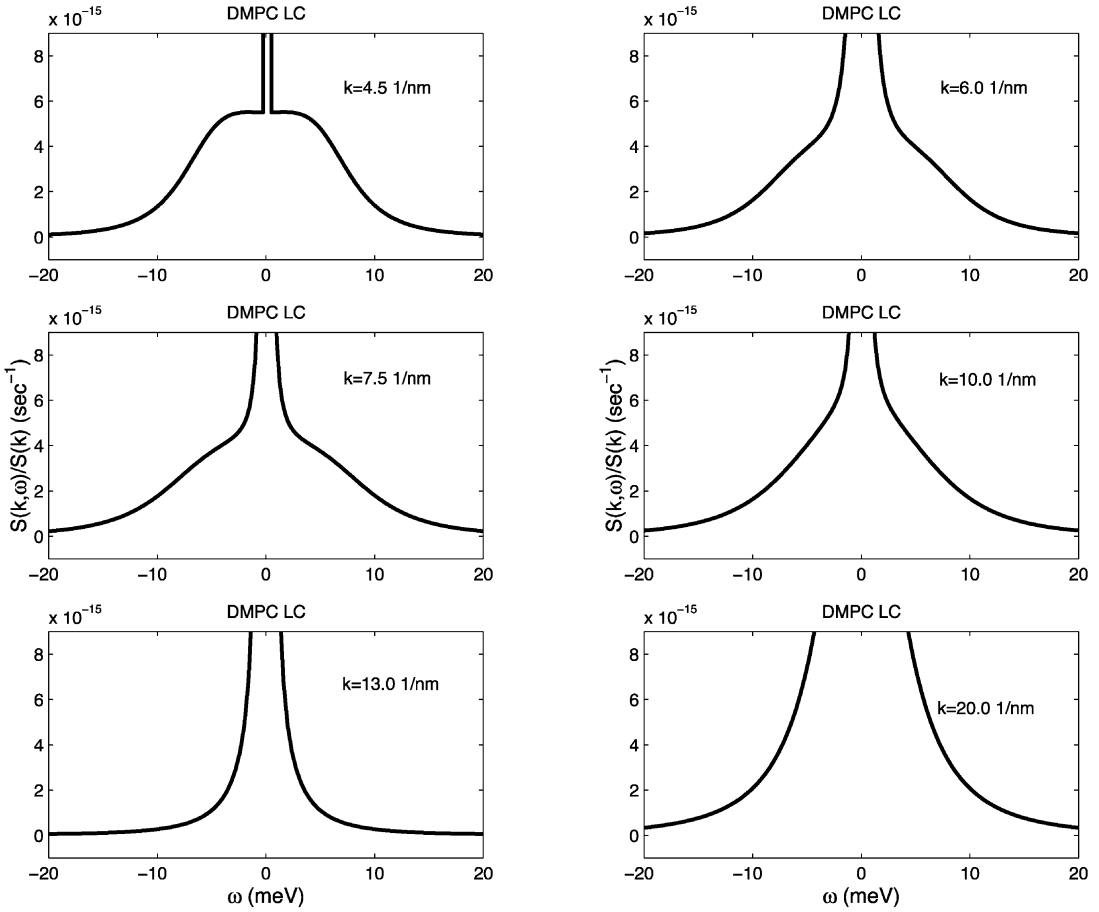

Fig. 3. The evolution of $S(k,\omega)$ for DMPC in the liquid crystal phase at $T=308$ K, as a function of ω at different k values, extracted from experimental IXS spectra, is shown using the GTEE model. Although the general shape of the spectra is similar to that in the gel phase, it should be noted that the phonon peaks are less well defined, because in the liquid crystal phase, the lipid molecules are not ordered in the bilayer plane.

the denominator $-z^3+(z_u+z_T)z^2-(z_uz_T+f_{uT}^2+f_{un}^2)z+f_{un}^2z_T$ as $-Q(z)$. In most of the cases, the roots of the equation $Q(z)=0$ consist of one real number Γ_h and a couple of conjugate complex number $\Gamma_s\pm i\Omega_s$ and the Eq. (23) can be factorized in the following form

$$S(k,z)/S(k)=\frac{1}{\pi}\left\{\frac{P(z)}{Q(z)}\right\}=\left\{\frac{A(z)}{z-\Gamma_h}+\frac{(B+Cz)}{(z-\Gamma_s)^2+\Omega_s^2}\right\} \tag{24}$$

where $A(z)=\dfrac{P(z)}{Q'(z)}$, $B=-2\Gamma_s\mathrm{Re}\left(\dfrac{P(\Gamma_s+i\Omega_s)}{Q'(\Gamma_s+i\Omega_s)}\right)-2\omega_s\mathrm{Im}\left(\dfrac{P(\Gamma_s+i\Omega_s)}{Q'(\Gamma_s+i\Omega_s)}\right)$, and $C=2\mathrm{Re}\left(\dfrac{P(\Gamma_s+i\Omega_s)}{Q'(\Gamma_s+i\Omega_s)}\right)$. One can therefore cast the normalized dynamic structure factor in a hydrodynamic-like form

$$S(k,\omega)/S(k)=\frac{1}{\pi}\left\{A_0\frac{\Gamma_h}{\omega^2+\Gamma_h^2}+A_s\frac{\Gamma_s+b(\omega+\Omega_s)}{(\omega+\Omega_s)^2+\Gamma_s^2}+A_s\frac{\Gamma_s-b(\omega-\Omega_s)}{(\omega-\Omega_s)^2+\Gamma_s^2}\right\} \tag{25}$$

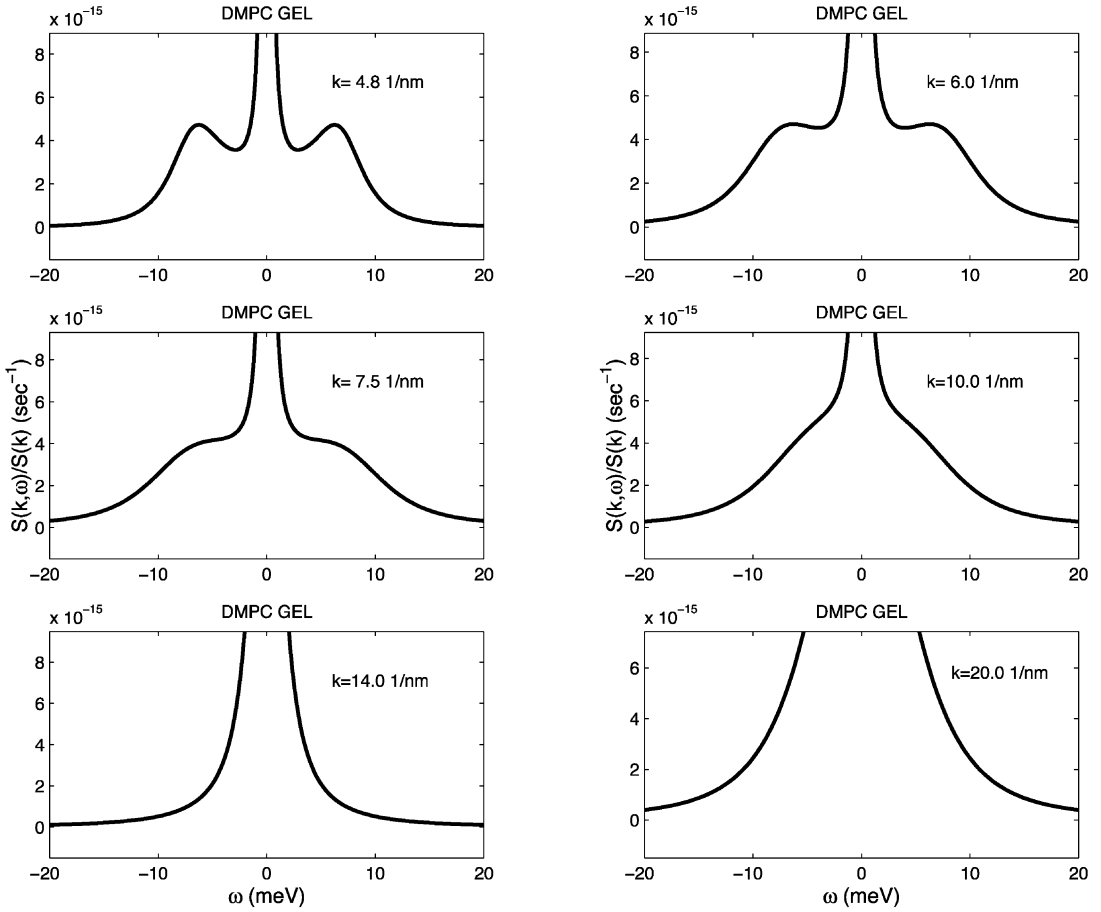

Fig. 4. The evolution of $S(k,\omega)$ for DMPC in gel phase at $T=293$ K, as a function of ω at different k values, extracted from experimental IXS spectra, is shown using the GTEE model. It can be seen that up to $k=7.5$ nm^{-1} which is the location of the first peak of the dispersion relation, the phonon peaks are well defined. At large k, although the phonon peak is not clearly seen in the spectrum, nevertheless, according to GTEE theory, it is still possible to decompose the spectra into three overlapping Lorentzian peaks, one central and two symmetric side peaks. Hence, one can still assign a phonon frequency and its damping. The concept of phonon ceases to exist when the three Lorentzian peaks all center around $\omega=0$. It is interesting to note that at $k=14.0$ nm^{-1}, which is the position of the peak of the static structure factor $S(k)$, one can clearly see the so-called DeGenne narrowing of the spectrum.

where

$$M(x)=x^2-(z_u+z_T)x+z_uz_T+f_{uT}^2,$$
$$N=\frac{M(\Gamma_s-i\Omega_s)}{2i\Omega_s(\Gamma_h-(\Gamma_s-i\Omega_s))}$$
$$A_0=\frac{M(\Gamma_h)}{(\Gamma_s-\Gamma_h)^2+\Omega_s^2},$$
$$A_s=\mathrm{Re}(N),$$
$$b=-\mathrm{Im}(N)/\mathrm{Re}(N). \quad (26)$$

According to Eq. (25), the three poles of $S(k,z=i\omega)$ are Γ_h and $\Gamma_s\pm i\Omega_s$, respectively, where $\Gamma_h(k)$ is the relaxation rate of the central non-propagating mode, $\Gamma_s(k)$ is the damping, and Ω_s is the frequency of the high frequency sound (phonon) mode. These three physical parameters are functions of the four fitting parameters: $f_{un}(k)$, $z_u(k)$, $f_{uT}(k)$ and $z_T(k)$. In the hydrodynamic limit $k\to 0$, the parameters in Eq. (25) satisfy $A_0=[(\gamma-1)/\gamma]$, $A_s=1/2\gamma$, $\Omega_s=c_sk$, $\Gamma_h=D_Tk^2$ and $\Gamma_s=\alpha k^2$, where c_s is the adiabatic sound speed, D_T the

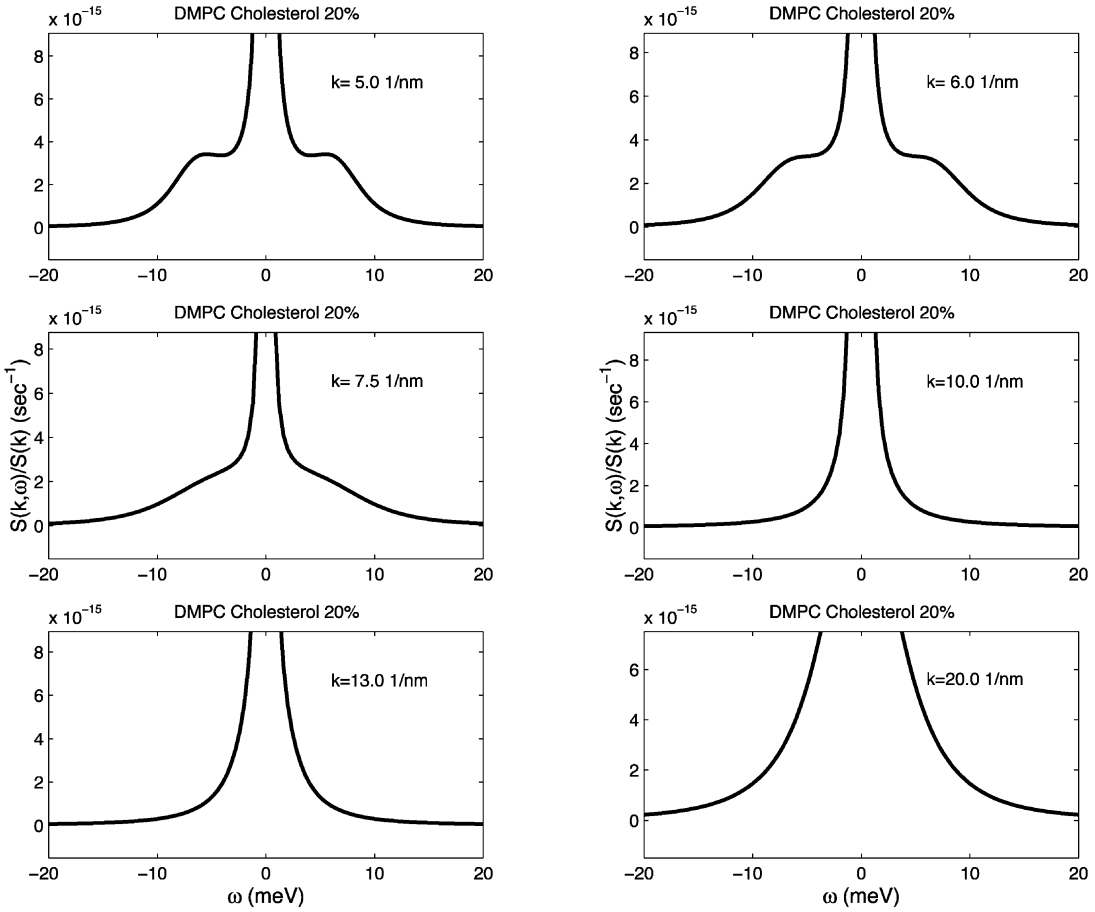

Fig. 5. The evolution of $S(k,\omega)$ for DMPC with addition of 20% cholesterol at $T=308$ K, as a function of ω at different k values, extracted from experimental IXS spectra, is shown using the GTEE model. We can see that the phonon peaks of the spectra are in general better defined compared to those in the liquid crystal phase. One can argue that the insertion of cholesterol molecules increases the stiffness of the bilayer. Thus, the bilayer becomes more solid-like and hence the propagating phonon modes become more well defined.

thermal diffusivity, $\alpha=(1/2)[v+(\gamma-1)D_T]$ the sound damping factor, $\gamma=\dfrac{C_p}{C_v}$ the specific heat ratio, and v is the kinematic longitudinal viscosity.

We can also cast the GTEE model in the form of a continued fraction expansion,

$$S(k,z=i\omega)=\left[z+\frac{f_{un}^2(k)}{z+z_u(k)+\dfrac{f_{uT}^2(k)}{z+z_T(k)}}\right]^{-1}. \qquad (27)$$

From this expression, the second-order memory function of the spectral density of the density–density correlation function can be seen to be of the form:

$$K_L(k,z=i\omega)=z_u(k)+\frac{f_{uT}^2(k)}{z+z_T(k)} \qquad (28)$$

Eq. (28) is useful for comparison with other theories formulated in terms of the memory function.

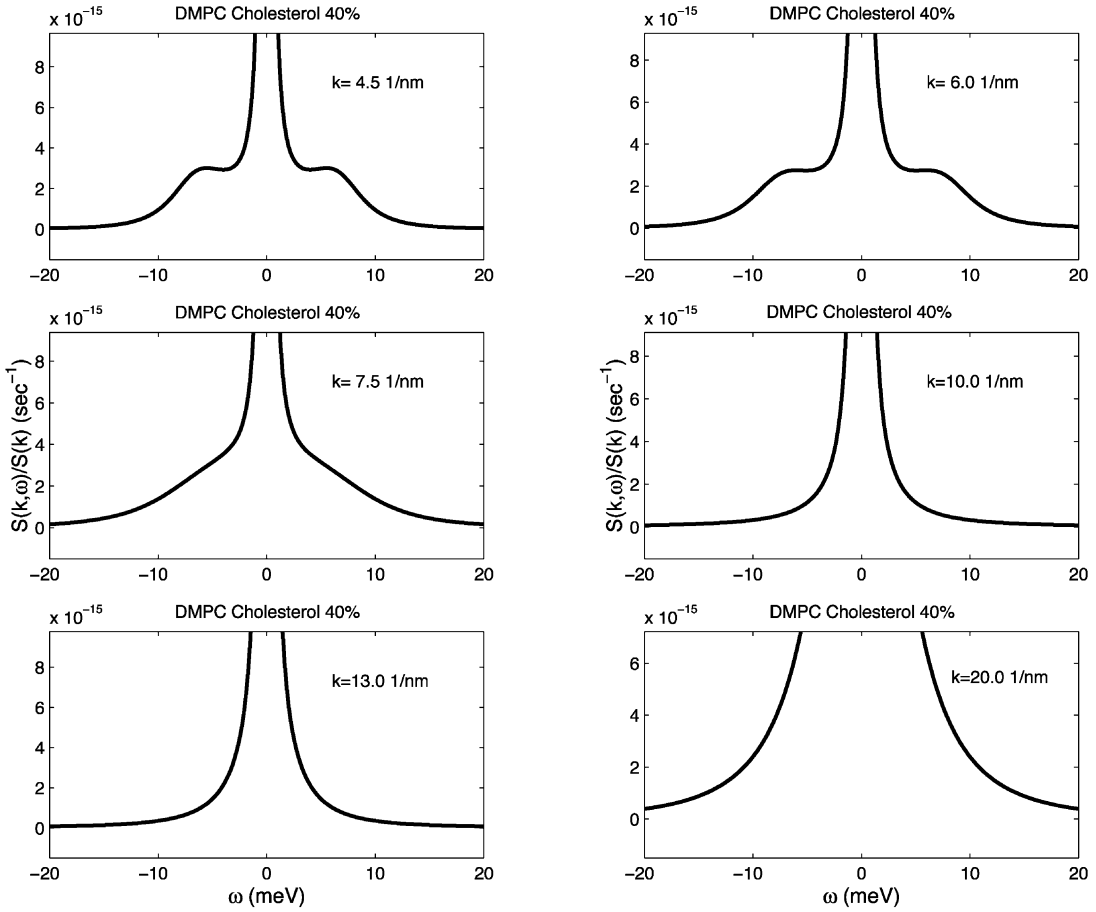

Fig. 6. The evolution of $S(k,\omega)$ for DMPC with addition of 40% cholesterol at $T=308$ K, as a function of ω at different k values, extracted from experimental IXS spectra, using the GTEE model. The side peaks of the spectra are slightly sharper, otherwise similar to the case of DMPC with 20% cholesterol added. We can reconfirm our previous observation that the addition of the cholesterol molecules stiffen the bilayer.

To fit the IXS data, we use the four adjustable parameters in Eq. (23) among which f_{un} can be compared with static structure factor $S(k)$ using Eq. (20). The theoretical dynamic structure factor is then multiplied by the Bose factor (the detailed balance factor) and convoluted with the energy resolution function before compared with experimental spectrum, which has been normalized to have unit area. Fig. 2 shows the normalized IXS spectrum $S(k,\omega)/S(k)$, in unit of s^{-1}, of DMPC bilayer in the gel phase at $T=293$ K at $k=4.8$ nm^{-1} fitted with the GTEE model. The theoretically calculated dynamic structure factor is indicated by the solid line and the dotted line represents the energy resolution function. The convolution of the theoretical dynamic structure factor (multiplied by the Bose factor) with the energy resolution function is given in a thick solid line which goes through all the experimental points (symbols). The χ^2 of the fit is of the order of unity. The result of the fit gives values of the three physical parameters shown also in the figure: $\Omega_s=$ 7.071 meV, $\Gamma_h=0.030$ meV and $\Gamma_s=3.029$ meV, respectively. The fitting of the spectra for other k

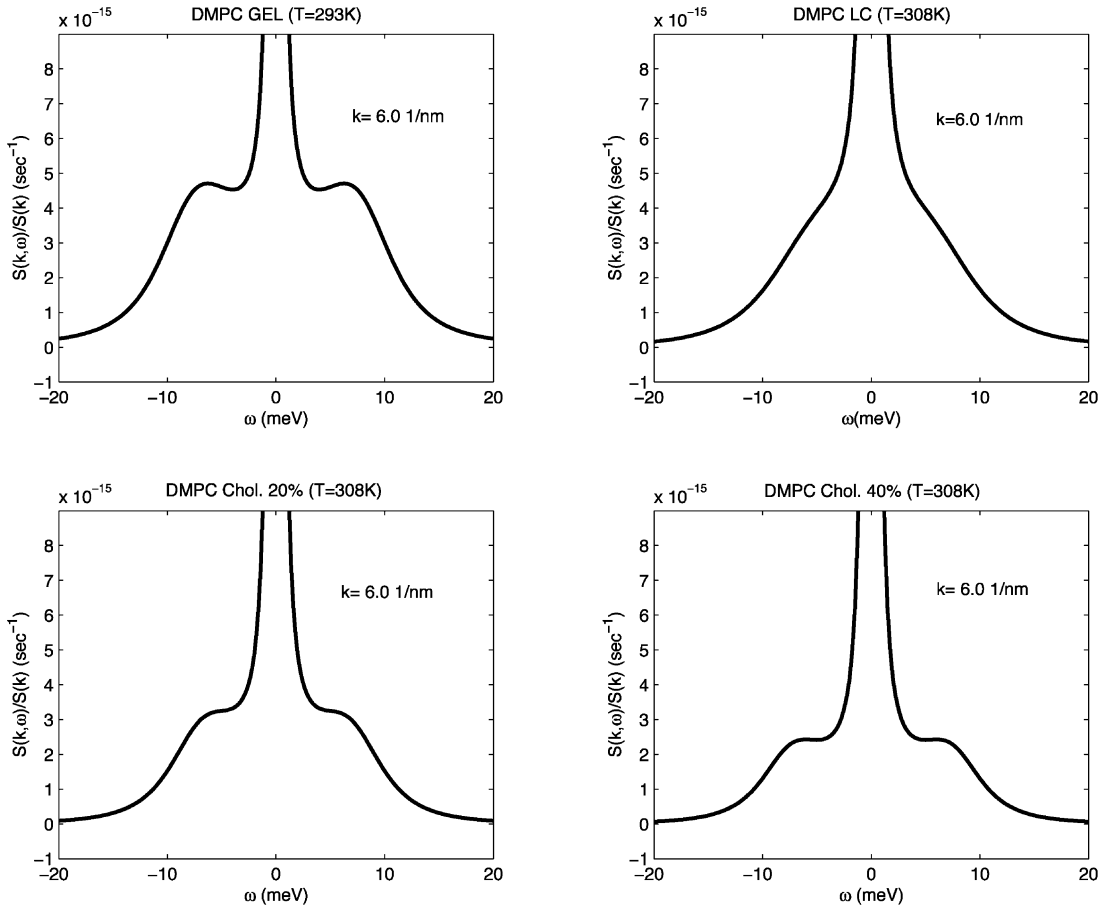

Fig. 7. A comparison of four $S(k,\omega)$ all taken at $k=6$ nm^{-1} for the four different cases are presented above. It illustrates the point that the two samples with cholesterol added have dynamic structure factors closer to the case of DMPC in the gel phase than to that of DMPC in the liquid crystal phase.

values in general shows good agreement with the experimental data, giving the χ^2 in the range of 1–6.

4. Results and discussion

The GTEE model is a powerful tool for analysis of IXS spectra in a fluid medium. From the GTEE model analysis, we obtain the following information from the spectrum: the dynamic structure factor $S(k,\omega)$, the phonon dispersion relation $\Omega_s(k)$ as a function of k; the phonon damping $\Gamma_s(k)$ as a function of k; and relaxation rate of the central mode $\Gamma_h(k)$ as a function of k.

In Figs. 3–6, we show $S(k,\omega)$ as a function of ω at different k values, extracted from experimental IXS spectra, using the GTEE model for DMPC in the liquid crystal phase at $T=308$ K, in the gel phase at $T=293$ K, with addition of 20% (mole percent) cholesterol at $T=308$ K and with addition of 40% (mole percent) cholesterol at $T=308$ K, respectively. It can be seen in these figures that at low k, the dynamic structure factor consists of three modes, a sharp central mode, and two symmetric, broad side peaks representing the high frequency sound mode or the phonon mode. In the case of light scattering, the central mode is called the Rayleigh peak and the side peaks are called

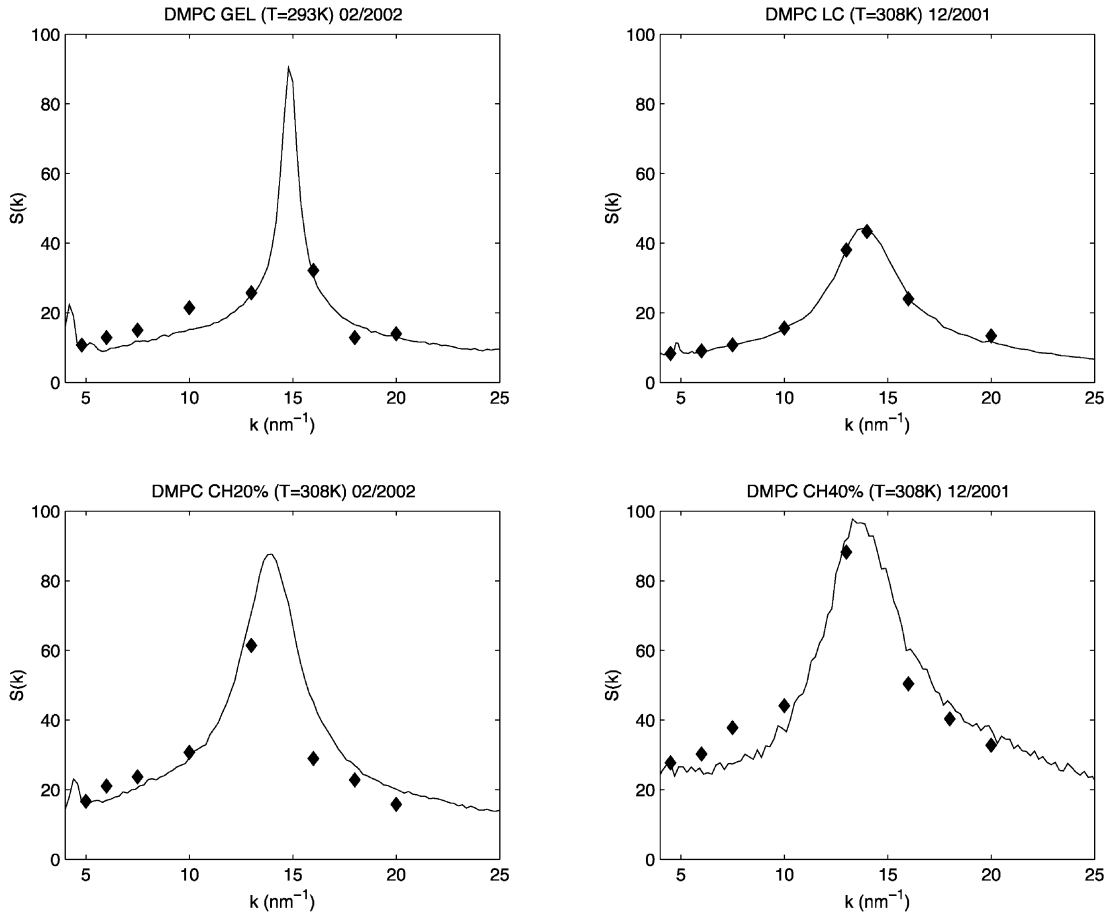

Fig. 8. The static structure factors in the region of the lipid–lipid correlation peak, which is located at approximately $k=15$ nm^{-1}. Our IXS measurements span a k range from 4.5 to 20 nm^{-1}, including this peak. In order to test the goodness of fit of the GTEE theory, we compare the absolute value of the structure factor deduced from one of the fitting parameters, $f_{un}(k)$. These theoretical structure factors as a function of k are shown by solid diamonds while the measured structure factors are given as the solid lines. Since the measured structure factor is in an arbitrary scale, in order to compare with the fitted $S(k)$, we have to normalize the measured one by a constant scale factor. It is seen that an agreement between the experimental and theoretical structure factors is satisfactory, indicating that the fitting procedure is sound.

the Brillouin peaks. $S(k,\omega)$ measured by IXS is thus an extension of the Rayleigh–Brillouin triplet measured in a conventional light scattering experiment to the higher k values (or short wavelength, $\lambda=2\pi/k$). For the liquid crystal phase in Fig. 3, we see that the phonon peaks are well defined up to $k=7.5$ nm^{-1}, which is the location of the first peak of the dispersion relation. At large k, although the phonon peak is not clearly seen in the spectrum, nevertheless, according to the GTEE theory, it is still possible to decompose the spectra into three overlapping Lorentzian peaks, one central and two symmetric side peaks. Hence, one can still assign a phonon frequency and its damping. The concept of phonon ceases to exist when the three Lorentzian peaks all center around $\omega=0$. It is interesting to mention that at $k=13.0$ nm^{-1} (see Fig. 8) which is the position near the peak of the static structure factor $S(k)$ one can clearly see the so-called DeGennes narrowing [37] of the spec-

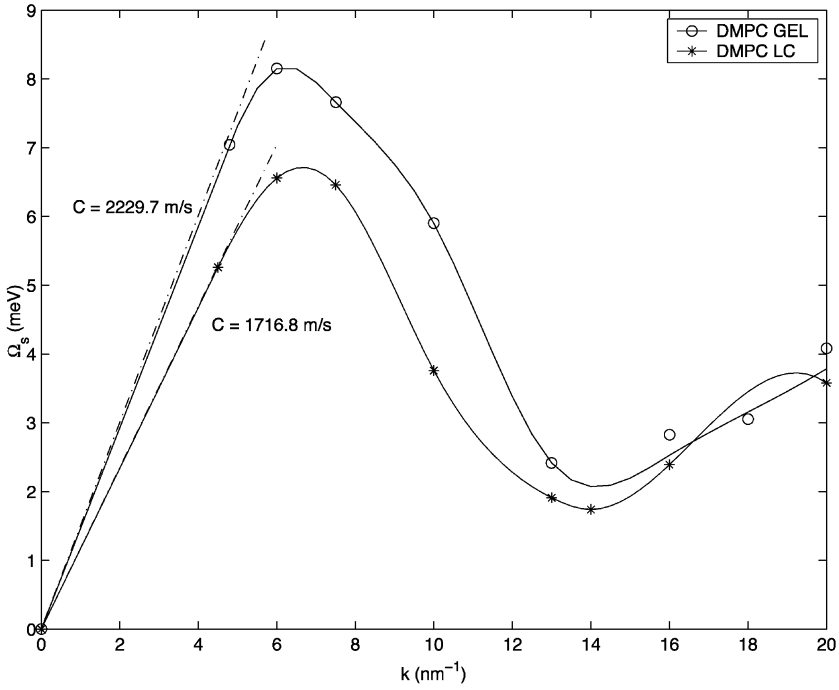

Fig. 9. The in-plane phonon dispersion relations of DMPC bilayer at two temperatures, corresponding to the gel and liquid crystal phases, respectively, of the bilayer. From the figure, we can see that the dispersion relations are structure dependent, i.e. the in-plane collective oscillations of the hydrocarbon chains also depend on the order of the lipid molecules in the bilayer plane. In the gel phase ($T=293$ K), the hydrocarbon chains are ordered, so the phonon frequency and the sound speed is higher. In the liquid crystal phase ($T=308$ K) because the chains are disordered, the phonon frequency and the sound speed are lower. It should be noted that the frequency gap at $k=14.0$ nm^{-1} is also smaller for the liquid crystal case.

trum. For the gel phase in Fig. 4, although the general shape of the spectra is similar to that in the liquid crystal phase, it should be noted that the phonon peaks are more well defined, because in the gel phase, the lipid molecules are more ordered in the bilayer plane. Fig. 5 shows the case for DMPC with addition of 20% (mole percent) cholesterol at $T=308$ K. In general, we can see that the phonon peaks of the spectra are better defined compared to those in the liquid crystal phase. One can argue that the insertion of cholesterol molecules into a bilayer increases the stiffness of the bilayer [26]. Thus, the bilayer becomes more solid-like and hence the propagating phonon modes become more well defined. Fig. 6 is the result from DMPC with addition of 40% cholesterol at $T=308$ K. The side peaks of the spectra are slightly sharper, otherwise similar to the case of DMPC with 20% cholesterol added. We can reconfirm our previous observation that the addition of the cholesterol molecules stiffens the bilayer.

Fig. 7 gives a comparison of four $S(k,\omega)$ all taken at $k=6$ nm^{-1} (near the peak position of the phonon dispersion relation) for the four different cases presented above. It illustrates the point that the two samples with cholesterol added have dynamic structure factors closer to the case of DMPC in the gel phase than to that of DMPC in the liquid crystal phase.

In order to test the goodness of the fit of the GTEE theory to the measured spectrum, we compare the absolute value of the structure factor deduced from one of the fitting parameters, $f_{un}(k)$, with the measured static structure factor. Fig. 8 shows the static structure factors in the region of the lipid–lipid correlation peak, which is located

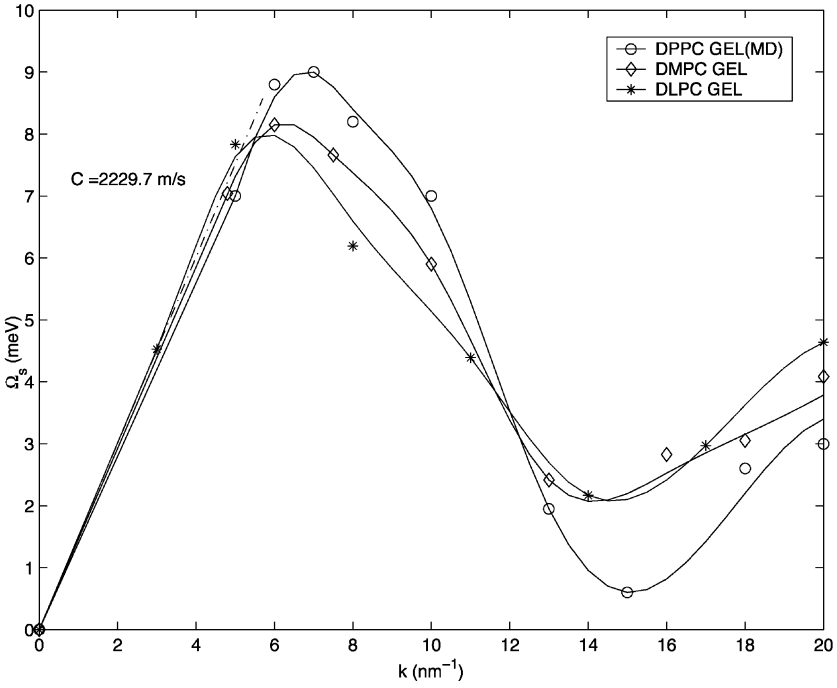

Fig. 10. The comparison of the in-plane phonon dispersion relations of DLPC and DMPC bilayers in the gel phase ($T=293$ K) from IXS experiments and DPPC in the gel phase ($T=293$ K) from MD simulations, respectively. An interesting feature to note is that as the lipid chain length increases, the phonon frequency at $k=7.0$ nm^{-1} (the peak of the dispersion relation) increases, on the other hand the one at $k=14.0$ nm^{-1} (the valley of the dispersion relation) decreases.

near $k_{\max}=14-15$ nm^{-1} (corresponding to the lipid–lipid head group distance $d=\frac{2\pi}{k_{\max}}\approx 0.4$ nm). Our IXS measurements span a k range from 4.5 to 20 nm^{-1}, including this peak. The theoretical structure factors as a function of k are shown by solid diamonds while the measured structure factors are given as the solid lines. Since the measured structure factor is in an arbitrary scale, in order to compare with the fitted $S(k)$, we have to normalize the measured one by a constant scale factor. It is seen that an agreement between the experimental and theoretical structure factors is satisfactory, indicating that the fitting procedure is sound.

The in-plane phonon dispersion relations of DMPC bilayer at two temperatures, corresponding to the gel and liquid crystal phases, respectively, of the bilayer are shown in Fig. 9. From the figure, we can see that the dispersion relations are structure dependent, i.e. the in-plane collective oscillations of the hydrocarbon chains also depend on the order of the lipid molecules in the bilayer plane. In the gel phase ($T=293$ K), the hydrocarbon chains are ordered, so the phonon frequency and the sound speed are higher. In the liquid crystal phase ($T=308$ K) because the chains are disordered, the phonon frequency and the sound speed are lower. We note that the existence of the valley at $k=14$ nm^{-1} is similar but more pronounced than that in the simple liquids.

The examples are the gap in the dispersion curves in liquid argon [41], the Lennard–Jones fluid, and the dips in liquid cesium [45] and liquid He^4 [46]. One can make a qualitative argument as to why the dispersion relation has a valley at the peak of the structure factor. One knows that the second moment of normalized dynamic structure factor is given by $\langle\omega^2\rangle=k^2v_0^2(k)/S(k)$, assuming that the dynamic structure factor consists of a sharp triplet with a central peak and symmetrically

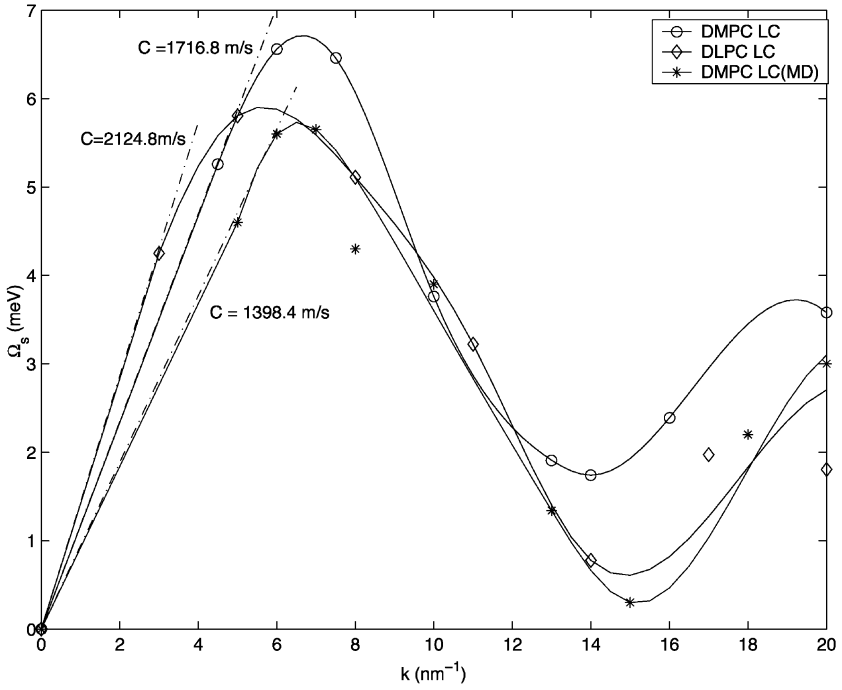

Fig. 11. The comparison of the in-plane phonon dispersion relations of DMPC ($T=308$ K) and DLPC ($T=294$ K) bilayers in the liquid crystal phase from IXS experiments and DMPC ($T=308$ K) bilayer in the liquid crystal phase from MD simulations. Although the phonon frequencies in DMPC (experiment) are higher than that of the DLPC (experiment), the same pattern noted in the last figure, the MD result seems to be lower than the corresponding IXS data. This discrepancy is judged to be more than the error bars of the fittings.

shifted side peaks located at $\pm\Omega_s$. Then the second moment is dominated by the shifted peaks and is approximately equal to $2\Omega_s^2$. Hence, we have an approximate relation that the sound frequency

$$\Omega_s = kv_0(k)/\sqrt{2S(k)}, \tag{29}$$

i.e. Ω_s is inversely proportional to the square root of the structure factor. This argument although plausible is, however, not quantitatively accurate except for the position of the minimum. This is because the argument does not take into account the finite damping of the central and side peaks. For the lipid bilayer, the dip in the dispersion relation is actually deeper in the liquid crystal phase than in the gel phase, while the experimental structure factor peak is lower in the former than in the latter as can be seen from Fig. 8.

We present a series of comparisons of the in-plane phonon dispersion relations for different samples from IXS measurements and MD simulations. Fig. 10 is the comparison of the in-plane phonon dispersion relations of DLPC and DMPC bilayers in the gel phase ($T=293$ K) from IXS experiments and DPPC in the gel phase ($T=293$ K) from MD simulations, respectively. An interesting feature to note is that as the lipid chain length increases, the phonon frequency at $k=7.0$ nm^{-1} (the peak of the dispersion relation) increases, on the other hand, the one at $k=14.0$ nm^{-1} (the valley of the dispersion relation) seems to decrease. However, the latter conclusion is highly uncertain because the measured spectrum at the peak of the structure factor is nearly as narrow as the resolution function. So the GTEE model analysis becomes very difficult and the resultant phonon frequency highly uncertain. Fig. 11 is the

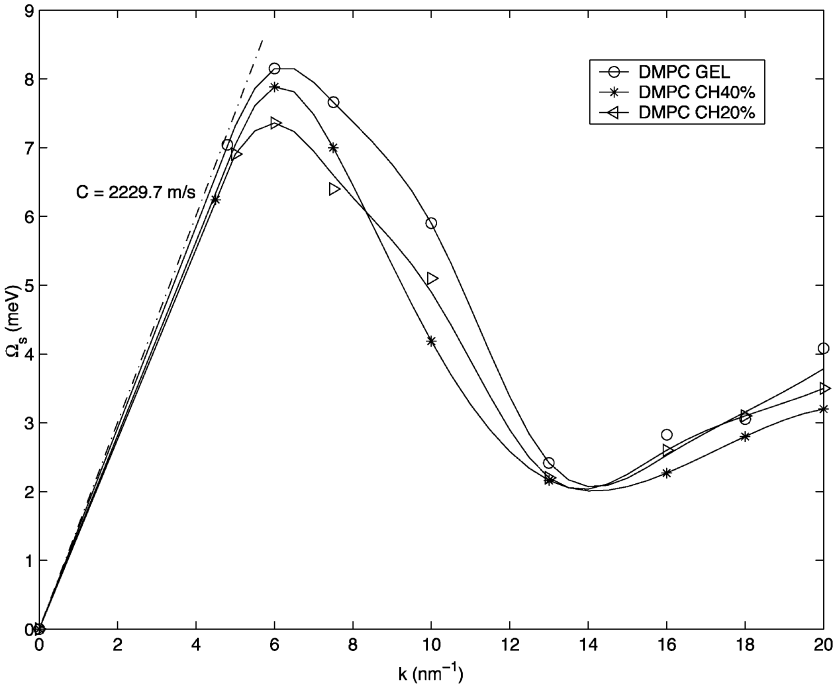

Fig. 12. The comparison of phonon dispersion relations of DMPC in the gel phase ($T=293$ K), DMPC with 40 and 20% cholesterol content at $T=308$ K. In spite of the fact that at $T=308$ K, a pure DMPC bilayer would be in the liquid crystal phase, but with the addition of cholesterol molecules, both phonon frequencies and the sound speed come close to the DMPC bilayer in the gel phase at $T=293$ K. This clearly shows that the effect of addition of cholesterol molecules is to make the bilayer more rigid, thus blurs the distinction between the liquid crystal and gel phases of the bilayer.

comparison of the in-plane phonon dispersion relations of DMPC ($T=308$ K) and DLPC ($T=294$ K) bilayers in the liquid crystal phase from IXS experiments and DMPC ($T=308$ K) bilayer in the liquid crystal phase from MD simulations. Although the phonon frequencies in DMPC (experiment) are higher than that of the DLPC (experiment), the same pattern noted in the last figure, the MD result for DMPC does not seem to agree with the IXS experimental data of DMPC. Fig. 12 is the comparison of phonon dispersion relations of DMPC in the gel phase ($T=293$ K), DMPC with 40 and 20% cholesterol content at $T=308$ K. In spite of the fact that at $T=308$ K, a pure DMPC bilayer would be in the liquid crystal phase, but with the addition of cholesterol molecules, both phonon frequencies and the sound speed come close to the DMPC bilayer in the gel phase at $T=293$ K. This clearly shows that the effect of addition of cholesterol molecules is to make the bilayer more rigid, thus blurs the distinction between the liquid crystal and gel phases of the bilayer. It is known in the literature [26,25,47], the addition of a substantial amount of cholesterol to DPPC membranes will result in a new phase called the liquid order phase which is different from the gel and liquid crystal phases exhibiting the properties of a liquid and solid.

The k dependence of the ratio of phonon damping to its frequency for DLPC, DMPC at $T=293$ K (gel phase) and DMPC at $T=308$ K with 20 and 40% cholesterol addition is shown in Fig. 13. It is seen that at low k values, damping is a fraction of the frequency but at high k values it can become larger than the frequency. Fig. 14 shows k dependence of the relaxation rate $\Gamma_h(k)$ of the central mode of the dynamic structure factor. The relaxation rate has a quadratic dependence on

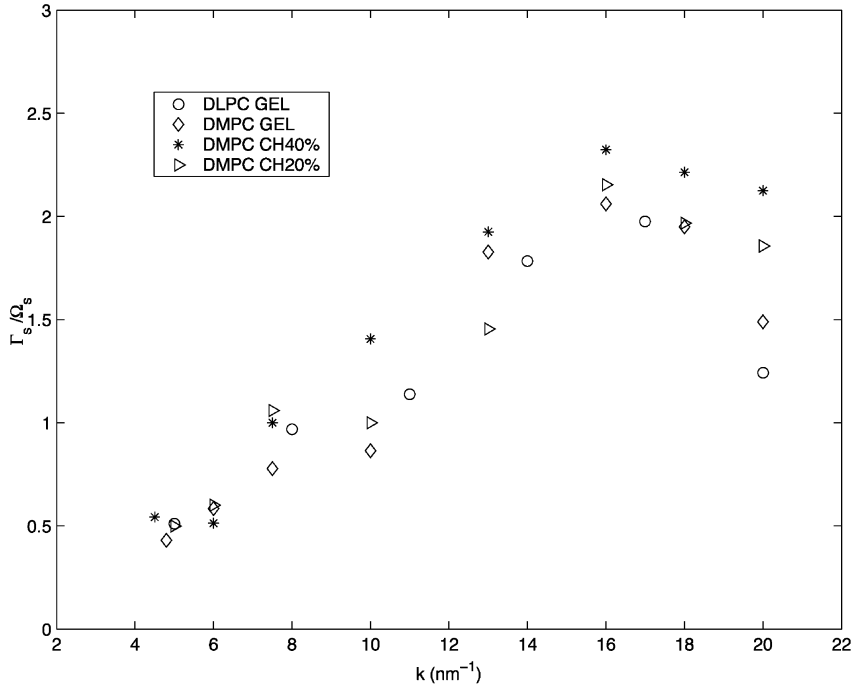

Fig. 13. The k dependence of the ratio of phonon damping to its frequency shows that at low k, damping is a fraction of the frequency but at high k it can become bigger than the frequency.

k with a proportionality constant, which is the thermal diffusivity D_T. Quadratic fit to all the data gives $D_T = 7.6 \times 10^{-6}$ cm^2/s with a large experimental error bar.

5. Conclusions

We have summarized the result of IXS investigation of in-plane collective excitations in lipid bilayers composed of DLPC [19], DMPC and DMPC with the addition of cholesterol [33]. This in-plane collective excitation was conjectured as the longitudinal density oscillations of the center of mass of lipid, molecules as a whole by using MD simulations of DPPC and DMPC bilayers [20]. Specifically, we have presented the detail of the analysis method, called the GTEE model, which allows us to extract the following physical quantities: the dynamic structure factor $S(k,\omega)$; the phonon dispersion relation, $\Gamma_s(k)$ as a function of k; the phonon damping $\Gamma_s(k)$ as a function of k; and relaxation rate of the central mode $\Gamma_h(k)$ as a function of k. We compare these extracted quantities as a function of lipid chain length, its two different main phases, liquid crystal vs. gel phases, and the effect of the addition of cholesterol to the bilayer. Followings are our main findings:

1. The general feature of the dispersion relation for phonons in a bilayer is that it increases linearly for small k values, reaching a peak and then comes down to a valley at $k_{\max}$ corresponding to the peak of the static structure factor $S(k)$. The peak of the dispersion relation occurs at approximately one half of $k_{\max}$. Occurrence of the valley in the dispersion relation can be understood from the known second frequency moment of the dynamic structure factor $S(k,\omega)$. We showed that phonon frequency Ω_s as a function of k is inversely proportional to the square root of the static structure factor $S(k)$. The phonon frequency at $k_{\max}$ corresponds to the vibrational frequency of the two neighboring lipid molecules against each other. The fact that

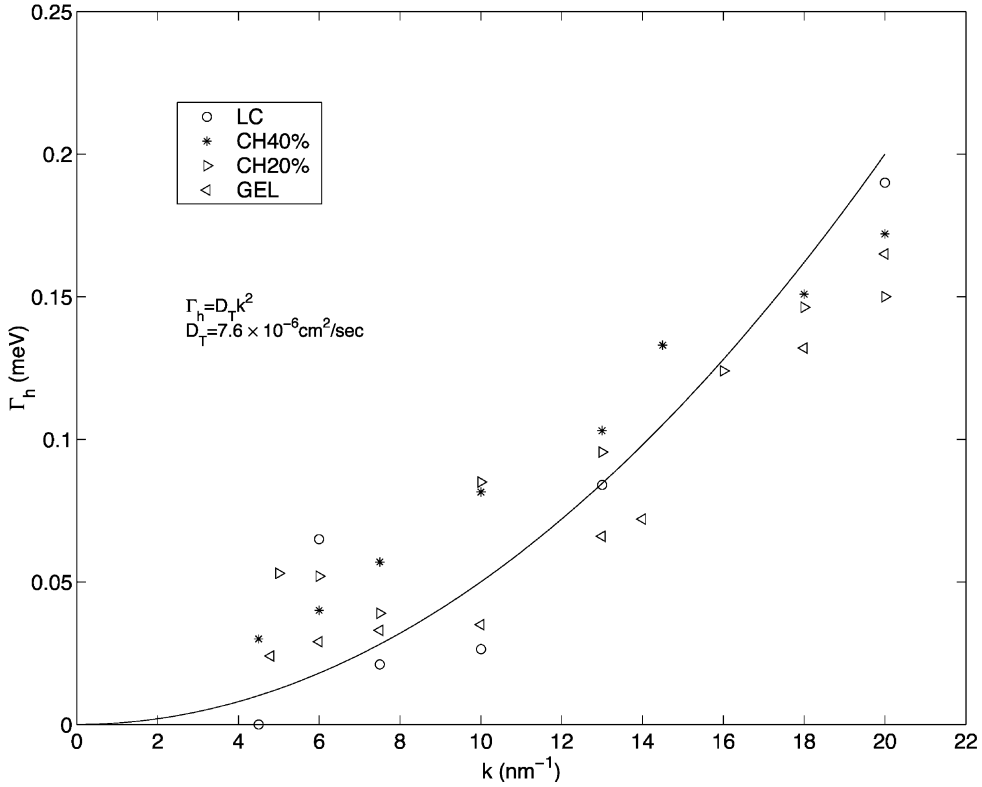

Fig. 14. The k dependence of the relaxation rate $\Gamma_h(k)$ of the central mode of the dynamic structure factor is shown. The relaxation rate has a quadratic dependence on k with a proportionality constant, which is the thermal diffusivity D_T. Quadratic fit to the all the data gives $D_T=7.6\times10^{-6}$ cm^2/s.

this frequency is lower in the liquid crystal phase than in the gel phase may have biological implication for mechanism of transport of small molecules across membranes.

2. Given the lipid chain length, the phonon frequencies and the high frequency sound speed are higher in the gel phase than in the liquid crystal phase due to the ordering of lipid molecules in the gel phase. The sound speed in the gel and liquid crystal phase are 2229.7 and 1716.8 m/s, respectively.
3. The phonon frequency at the peak of the dispersion relation increases with the chain length.
4. Addition of cholesterol molecules to DMPC, originally in the liquid crystal phase, has an effect of changing dynamic structure factor and the phonon dispersion relation closer to that of the gel phase. We interpret this result to mean that addition of cholesterol to the liquid crystal phase has a tendency of increasing the order of the lipid molecules in the bilayer, thus making the bilayer more solid-like.
5. The MD simulation result for DPPC in gel phase shows the right tendency for phonon frequencies as compared to the IXS result for DMPC and DLPC in gel phase. But MD result of dispersion relation for DMPC in liquid crystal phase shows some discrepancy with that of IXS result in DMPC.
6. The thermal diffusion constant is insensitive to the chain length and phases of the bilayer. It has a value $D_T=7.6\times10^{-6}$ cm^2/s, with a large error bar, for all the bilayers we studied.

We have demonstrated in this article that the high resolution inelastic X-ray scattering studies

of lipid bilayers have many potentials for offering new information in micro-mechanical properties of bilayers.

Acknowledgments

Research at MIT is supported by the Basic Sciences Division, Materials Research Program of US DOE. H.W.H. and T.M.W. are supported by grants from NIH and from Robert A. Welch Foundation. The research at APS is supported by US DOE BES Material Science contract No. W-31-109-ENG-38. PJC wishes to acknowledge financial support from a grant 2113-MIT-DOE-5912.

References

[1] R.D. Gennis, Biomembranes, Molecular Structure and Function, Springer-Verlag, New York, 1989.
[2] D.M. Small, The Physical Chemistry of Lipids, Plenum Press, New York, 1986.
[3] B.D. Ladbrooke, D. Chapmann, Chem. Phys. Lipids 3 (1969) 304.
[4] M.R. Morrow, P.J. Davis, C.S. Jackman, K.M. Keough, Thermal history alters cholesterol effect on transition of 1-palmitoyl- 2-linoleoyl phosphatidylcholine, Biophys. J. 71 (1996) 3207–3214.
[5] J. Seelig, Deuterium Magnetic-Resonance – Theory and Application to Lipid-membranes, Q. Rev. Biophys. 10 (3) (1977) 353–418.
[6] G. Buldt, H.U. Gally, A. Seelig, J. Seelig, Neutron-diffraction studies on selectively deuterated phospholipid bilayers, Nature 271 (1978) 182–184.
[7] F.Y. Chen, W.C. Hung, H.W. Huang, Critical swelling of phospholipid bilayers, Phys. Rev. Lett. 79 (1997) 4026–4029.
[8] W.J. Sun, R.M. Suter, M.A. Knewkson, C.R. Worthington, S. Tristram-Bagle, R. Zhang, et al., Order and disorder in fully hydrated unoriented bilayers of gel-phase dipalmitoylphosphatidylcholine, Phys. Rev. E 49 (1994) 4665–4676.
[9] K. Tu, D.J Tobias, M.L. Klein, Atomic-scale molecular dynamics simulations of lipid membranes, Curr. Opin. Colloid Interface Sci. 2 (1997) 15–26.
[10] K. Tu, D.J. Tobias, M.L. Klein, Constant pressure and temperature molecular dynamics simulation of a fully hydrated liquid crystal phase dipalmitoylphosphatidylcholine bilayer, Biophys. J. 69 (1995) 2558–2562.
[11] K. Tu, D.J. Tobias, K. Blasie, M.L. Klein, Molecular dynamics investigation of the structure of a fully hydrated gel-phase dipalmitoylphosphatidylcholine bilayer, Biophys. J. 70 (1996) 595–608.
[12] (a) P.F. Devaux, H.M. McConnell, J. Am. Chem. Soc. 94 (1972) 4475
(b) J.H. Sachse, M.D. King, D. Marsh, Unconstrained optimization method for interreting the concentration and temperature-dependence of the linewidths of interacting nitroxide spin labels – application to the measurement of translational diffusion-coefficients of spin-labelled phospholipids in membranes, J. Mag. Reson. 71 (1987) 257–267.
[13] M. Bloom, E.E. Burnell, A.L. Mackay, C.P. Nichol, M.F. Valic, G. Wekks, Fatty acyl chain order in lecithin model membranes determined from proton magnetic resonance, Biochemistry 17 (1978) 5750–5762.
[14] P. Meier, E. Ohmes, G. Kothe, Multipulse dynamic nuclear magnetic resonance of phospholipid membranes, J. Chem. Phys. 85 (1986) 3598–3614.
[15] H.J. Gala, W. Hartmann, U. Theilen, E. Sackmann, 2-Dimensional passive random-walk in lipid bilayers and fluid pathways in biomembranes, J. Membrane Biol. 48 (1979) 215.
[16] E. Wu, K. Jacobson, D. Papahadjopoulos, Lateral diffusion in phospholipid multibilayers measured by fluorescence recovery after photobleaching, Biochemistry 16 (1977) 3936–3941.
[17] S. Konig, W. Pfeiffer, T. Bayerl, D. Richter, E. Sackmann, Molecular-dynamics of lipid bilayers studies by incoherent quasi-elastic neutron scattering, J. Phys. II 2 (1992) 1589–1615.
[18] W. Pfeiffer, S. Konig, J.F. Legrand, T. Bayerl, D. Richter, E. Sackmann, Neutron spin-echo study of membrane undulations in lipid multibilayers, Europhys. Lett. 3 (1993) 457–462.
[19] S.H. Chen, C.Y. Liao, H.W. Huang, T.M. Weiss, M.C. Bellisent-Funel, F. Sette, Collective dynamics in fully hydrated phospholipid bilayers studied by inelastic X-ray scattering, Phys. Rev. Lett. 86 (2001) 740–743.
[20] M. Tarek, D.J. Tobias, S.-H. Chen, M.L. Klein, Short wavelength collective dynamics in phospholipid bilayers: a molecular dynamics study, Phys. Rev. Lett. 87 (2001) 238101.
[21] H.R. Shmeeda, E.B. Golden, Y. Barenholz, Membrane lipids and aging, in: M. Chinitzky (Ed.), Biomembranes-Structural and Functional Aspects, VCH, Weinheim, 1994.
[22] P. Meleard, C. Gerbeaud, T. Pott, L. Fernandez-Puente, I. Bivas, M.D. Mitov, et al., Bending elasticities of model membranes: influences of temperature and sterol content, Biophys. J. 72 (1997) 2616–2629.
[23] (a) H. Trauble, J. Membrane Biol. 4 (1971) 193
(b) S. Paula, A.G. Volkov, A.N. Van Hoek, T.H. Haines, D.W. Deamer, Permeation of protons, potassium ions, and small polar molecules through phospholipid bilayers as a function of membrane thickness, Biophys. J. 70 (1996) 339–348.
[24] T.X. Xiang, B.D. Anderson, Permeability of acetic acid across gel and liquid-crystalline lipid bilayers conforms

to free-surface-area theory, Biophys. J. 72 (1997) 223–237.
[25] M.R. Vist, J.H. Davis, Phase-equilibria of cholesterol dipalmitoylphosphatidylchline mixtures: H-2 nuclear magnetic-resonance and differential scanning calorimetry, Biochemistry 29 (1990) 451–464.
[26] M.J. Zyckermann, J.H. Ispen, O.G. Mouritsen, Cholesterol and Membrane Models. L.X. Finegold (Ed.), CRC Press Inc., Boca Raton, Florida.
[27] J.H. Ipsen, O. Mouritsen, M. Bloom, Relationship between lipid membrane area, hydrophobeic thickness and acyl-chain orientational order. The effect of cholesterol, Biophys. J. 57, 405–412.
[28] P.F. Almeida, W. Vaz, T. Thompson, Lateral diffusion in the liquid phases of dimyristoylphosphatidylcholine/cholesterol lipid bilayers: a free volume analysis, Biochemistry 31 (1992) 6739–6747.
[29] J.H. Ipsen, G. Karlstr?m, O. Mouritsen, H. Wermerstr?m, M. Zuckermann, Phase equilibria in the phosphatidylcholine-cholesterol system, Biochem. Biophys. Acta. 905 (1987) 162–172.
[30] R.R. Gabdoulline, G. Vanderkooi, C. Zheng, Comparison of the structures of dimyristoylphosphatidylcholine in the presence and absence of cholesterol by molecular dynamics simulations, J. Phys. Chem. 100 (1996) 15942–15946.
[31] D.J. Tobias, K. Tu, M. Klein, Atomic-scale molecular dynamics simulations of lipid membranes, Curr. Opin. Colloid Interface Sci. 2 (1997) 15–26.
[32] K. Tu, M. Klein, D. Tobias, Constant pressure molecular dynamics investigation of cholesterol effects in a DPPC bilayer, Biophys. J. 75 (1998) 2147–2156.
[33] T.M. Weiss, P.J. Chen, H.W. Huang, S.H. Chen, H. Sinn, E.E. Alp (to be published).
[34] H. Sinn, E.E. Alp, A. Alatas, J. Barraza, G. Bortel, E. Burkel, et al., An inelastic X-ray spectrometer with 2.2 meV energy resolution, Nucl. Instrum. Methods Phys. Res. A 467–468 (2001) 1545–1548.
[35] J.P. Boon, S. Yip, Molecular Hydrodynamics, McGraw-Hill, New York, 1980.
[36] J.P. Hansen, I.R. McDonald, Theory of Simple Liquids, Academic Press, London, 1986.
[37] U. Balucani, M. Zoppi, Dynamics of the Liquid State, Oxford, Clarendon, 1994.
[38] S.H. Chen, M. Kotlarchyk, Interaction of Photons and Neutrons with Matter, World Scientific, 1997.
[39] C.Y. Liao, S.H. Chen, Theory of the generalized dynamic structure factor of polyatomic molecular fluids measured by inelastic X-ray scattering, Phys. Rev. E 64 (2001) 021205.
[40] I.M. de Schepper, E.G.D. Cohen, C. Bruin, J.C. van Rijs, W. Montfrooij, L.A. de Graaf, Hydrodynamic time correlation functions for a Lennard-Jones fluid, Phys. Rev. A 38 (1988) 271.
[41] I.M. de Schepper, P. Verkerk, A.A. van Well, L.A. de Graaf, Short-wavelength sound modes in liquid argon, Phys. Rev. Lett. 50 (1983) 974.
[42] W. Montfrooij, I.M. de Schepper, E.G.D. Cohen, Dynamics in He at 4 and 8 K from inelastic neutron scattering, J. Low Temp. Phys. 105 (1996) 149.
[43] C.Y. Liao, S.H. Chen, F. Sette, Analysis of inelastic X-ray scattering spectra of low-temperature water, Phys. Rev. E 61 (2000) 1518–1526.
[44] International Tables for X-ray Crystallography (Reidel, Dordrecht, 1985), Vol. III.
[45] T. Bodensteiner, Chr. Morkel, W. Glaser, B. Dorner, Collective dynamics in liquid cesium near the melting point, Phys. Rev. A 45 (1992) 5709.
[46] W. Montfrooij, E.C. Svensson, I.M. de Schepper, E.G.D. Cohen, Effective eigenmode description of normal and superfluid He^4, J. Low Temp. Phys. 109 (1997) 577–623.
[47] T.P.W. McMullen, R.N. McElhaney, New aspects of the interaction of cholesterol with dipalmitoylphosphatidylcholine bilayers as revealed by high-sensitivity differential scanning calorimetry, Biochim. Biophys. Acta 1234 (1995) 90–98.